Analysis of metallic impurities during the application of three-ion ICRH scenario at JET-ILW

Cite as: AIP Conference Proceedings **2254**, 050005 (2020); https://doi.org/10.1063/5.0013561
Published Online: 16 September 2020

A. Chomiczewska, N. Krawczyk, Ye. O. Kazakov, et al.

Analysis of Metallic Impurities During the Application of Three-ion ICRH Scenario at JET-ILW

A. Chomiczewska[1, a)], N. Krawczyk[1], Ye. O. Kazakov[2], V. Bobkov[3], E. Kowalska-Strzęciwilk[1], E. Lerche[2], M. J. Mantsinen[4], J. Ongena[2], G. Pucella[5], T. Pütterich[3], D. Van Eester[2] and JET Contributors

[1] *Institute of Plasma Physics and Laser Microfusion, Warsaw, Poland*
[2]*Laboratory for Plasma Physics, LPP-ERM/KMS, TEC Partner, Brussels, Belgium*
[3]*Max-Planck-Institut für Plasmaphysik, Garching, Germany*
[4]*ICREA-Barcelona Supercomputing Center, Barcelona, Spain,* [5]*ENEA, Fusion and Nuclear Safety Department, C. R. Frascati, Italy*
[a)]Corresponding author: agata.chomiczewska@ifpilm.pl

Abstract. The effect of the novel 'three-ion' D-(^{3}He)-H minority ICRH heating scheme on the behavior of the metallic impurities at JET-ILW is discussed. The reported experiment was performed in L-mode plasmas at a magnetic field B_T = 3.2 T, plasma current I_p = 2 MA and central plasma densities $n_e(0) \approx 4\times10^{19}$ m^{-3}. ICRH power was delivered with dipole or $+\pi/2$ antenna phasing at f ≈ 32.2-33MHz, placing the ^{3}He cyclotron resonance at the plasma core. The edge isotopic ratio H/(H+D) was varied between 73 and 92%, and ^{3}He concentration in the range of 0.1-1.5% to assess the sensitivity of the scheme to the detailed plasma composition. The results of our analysis show a linear increase of the plasma effective charge Z_{eff}, radiated power $P_{rad,bulk}$ and content of metallic impurities with ICRF power. The observed scattering of the points reflects the difference in the plasma composition and ICRF antenna phasing. For discharges heated with similar ICRH power level ~4MW, our analysis indicates that for a large range of H/(H+D) the novel scenario effectively heats the plasma with reduced content of metallic impurities. The impurities are shown to be concentrated mainly around the mid-radius region of the plasma. We conclude this paper with a discussion of the effect of the long-period sawteeth on the observed dynamics of metallic impurities in the plasma core.

INTRODUCTION

Ion cyclotron resonance heating (ICRH), in particular, H minority scheme in D plasmas, has been extensively used in recent experimental campaigns at JET with ITER-like wall (ILW). This ICRH scheme not only provides bulk plasma heating, but is also applied as a technique to prevent accumulation of heavy impurities. In H-mode plasmas optimization of (H)-D scheme for core impurity control in JET-ILW demonstrated a beneficial effect of applying ICRH with the H minority cyclotron resonance located as close to the plasma core as possible [1]. Recently, the high efficiency of a novel 'three-ion' minority ICRH scheme for plasma heating and fast-ion generation has been demonstrated on three tokamaks worldwide (Alcator C-Mod, AUG and JET-ILW) [2, 3]. The novel ICRH scenario requires a plasma including at least three ion species with a different ratio of the charge number to the atomic mass $(Z/A)_i$. The Z/A value for the resonant "third" species should be in between that of the two main ions i.e. $(Z/A)_2<(Z/A)_3<(Z/A)_1$. For proof-of-principle demonstration, the D-(^{3}He)-H scheme was chosen, which was applied for heating H-D mixed plasmas using ^{3}He ions as a minority. The novel scenario is characterized by an efficient absorption of RF power by a small amount of ^{3}He ions at the concentrations of the order of ~0.1-0.2 % with the H concentration in the range 70–80% [2]. In this paper, the effect of the D-(^{3}He)-H ICRH heating scheme on the behavior of the metallic impurities at JET-ILW is discussed.

EXPERIMENTAL RESULTS

The reported experiment was performed in L-mode JET-ILW plasmas at a magnetic field B_T = 3.2 T, plasma current I_p = 2 MA and central plasma densities $n_e(0) \approx 4\times10^{19}$ m^{-3}. The three-ion scenario was tested at RF frequency f ≈ 32.2-33MHz, placing the ^{3}He cyclotron resonance at the plasma core. ICRH power was delivered with dipole or $+\pi/2$ RF antenna phasing. Before the ICRH system was switched on, plasma was pre-heated with 3.2 MW of D-NBI

23rd Topical Conference on Radiofrequency Power in Plasmas
AIP Conf. Proc. 2254, 050005-1–050005-4; https://doi.org/10.1063/5.0013561
Published by AIP Publishing. 978-0-7354-2013-7/$30.00

power. This allowed to increase plasmas central electron temperature up to $T_e(0) \approx 2.6$ keV. Figure 1 shows the bulk radiated power $P_{rad,\,bulk}$ and the plasma effective charge Z_{eff} as a function of ICRH power applied. A linear increase of the parameters with ICRH power was observed. The obtained scattering of the points reflected the difference in the plasma composition and ICRH antenna phasing. The edge isotopic ratio H/(H+D) was varied between 73 and 92%, and ^{3}He concentration in the range of 0.1-1.5 %.

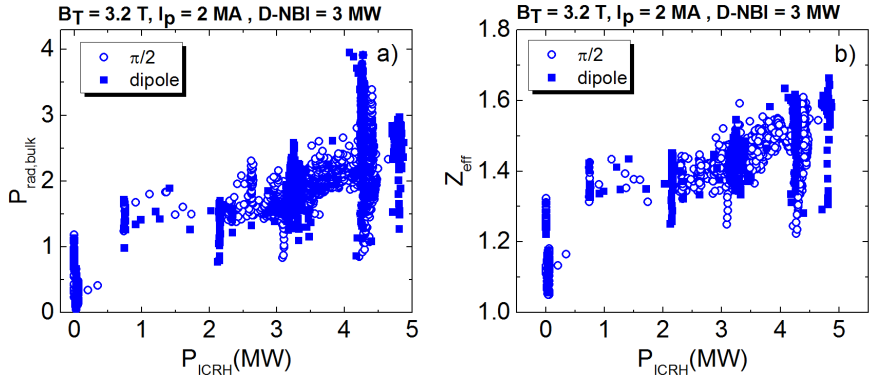

FIGURE 1. a) Bulk radiated power and b) Z_{eff} as a function of ICRH power in the JET three-ion D-(^{3}He)-H heating scenario. Squares correspond to pulses in which on-axis ICRH power was coupled with the dipole RF antenna phasing, while circles represent pulses with +π/2 phasing.

The dependence of impurity behavior in the chosen plasma composition was performed for similar ICRH power levels $P_{ICRH} \sim 4.0$ MW. The core hydrogen concentration $X[H]_{core}$ was estimated using the measured edge H/(H+D) ratio, corrected for the presence of impurities and additional core deuterium fueling from the D-NBI heating, resulting in $X[H]_{core} \approx 0.9 \times H/(H+D)$.

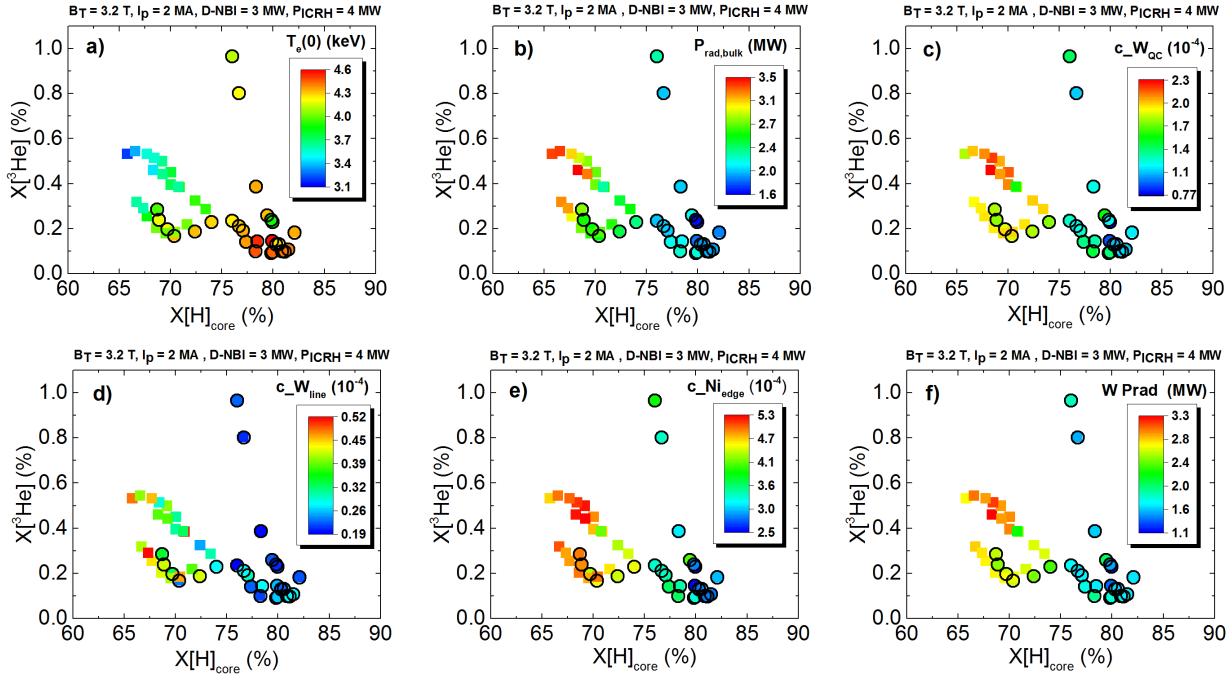

FIGURE 2. a) The central electron temperature b) bulk radiated power, c) W concentration calculated from W quasicontinuum at r/a~0.5 from XUV diagnostic, d) W concentration calculated from the W line radiation at r/a~0.2 from XUV diagnostic e) Ni concentration calculated from VUV diagnostic at r/a~0.8-0.9, f) W radiated power, as a function of the estimated core hydrogen and ^{3}He concentration in the JET three-ion D-(^{3}He)-H heating scenario. Squares correspond to ICRH with dipole phasing, while circles represent +π/2 ICRH phasing.

Figure 2a shows that at the concentrations of resonant minority ^{3}He ions of the order of ~0.2 % or even below, highest central electron temperature was achieved, indicating an efficient absorption of RF power in the three-ion ICRH scenario for a broad range of the isotopic ratio. At the same time reduced bulk radiated power was observed (see Fig. 2b). This was related to reduction of W and Ni impurity concentration (see Fig. 2c-e), which were the main intrinsic radiators. The W concentration defined as c_W_{QC} was estimated from the quasicontinuum (QC) emission at

wavelengths around 5 nm, measured by the JET XUV spectrometer looking from the top of the machine towards the JET divertor [4]. This spectral feature of the W-ions W^{27+} to W^{35+} was emitted at electron temperatures between 0.8-1.8 keV (r/a~0.5). The line radiation of W^{42+} to W^{45+} ions allowed to calculate c_W_{line}, which accounted for a more central W content (r/a~0.2). Higher values of c_W_{QC} in comparison to c_W_{line} presented in Fig. 2c, d indicated hollow W profile in the plasma center. The edge radiation was dominated by Ni ions, whose concentration presented in Fig. 2e was calculated based on the JET VUV spectroscopy data using the method described in [5]. The diagnostic has a horizontal line-of-sight looking at the vessel mid-plane. Similarly to W behaviour, Ni concentration was lower closer to the plasma center. As can be seen in Fig. 2f, W contributed to roughly 90 % of $P_{rad,bulk}$. By the fact that in these L-mode plasma no strong poloidal asymmetry was observed, information on the impurities from vertical and horizontal diagnostic lines-of-sight corresponds to the whole plasma.

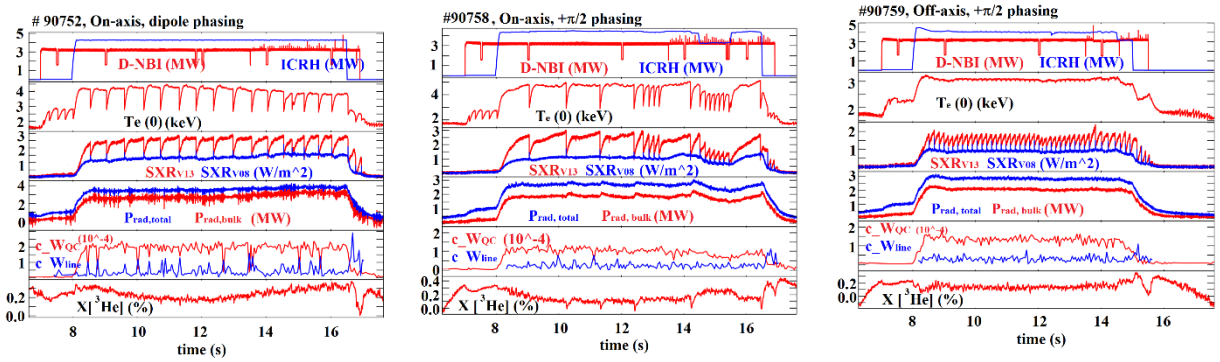

FIGURE 3. Time traces of the selected signals in JPN 90752 with on-axis ICRH power deposition and dipole antenna phasing, JPN 90758 with on-axis ICRH power deposition and +π/2 antenna phasing, and in JPN 90759 with off-axis ICRH power deposition and +π/2 antenna phasing. From the top: D-NBI and ICRH power, the central electron temperature from ECE diagnostic, plasma emission measurements from the vertical SXR camera channels close to the magnetic axis (SXR_{V13}) and close to the sawtooth inversion radius (SXR_{V8}), the total and the bulk radiated power from bolometry diagnostic, W concentration from quasicontinuum and line radiation measured by XUV diagnostic, ^{3}He concentration.

Figure 3 shows the time evolution of the central electron temperature T_e (0) in response to the applied ICRH power for two discharges in which RF power was deposited on-axis with dipole (JET Pulse Number JPN 90752) and +π/2 (JPN 90758) antenna phasing, and for discharge JPN 90759 with off-axis disposition and +π/2 antenna phasing. The electron temperature measurements from electron cyclotron emission (ECE) channels close to the magnetic axis was an indicator for the sawtooth crashes. A qualitative difference in sawtooth behaviour between the three discharges is apparent. In the case of on-axis heating and +π/2 phasing sawtooth period was longer than ~ 1s during the combined ICRH + NBI phase in comparison to dipole phasing with sawtooth period of ~500-600 ms. It appeared that by setting the resonance layer off-axis the shortest sawtooth period (~100-200 ms) was achieved. In all cases the sawtooth period was extended from ~ 200 ms during the NBI-only phase. It is common observation at JET that the sawteeth can be shortened with various antenna phasing and controlled with less accurate alignment between the resonance layer and the sawtooth inversion radius [6]. The excursions of the plasma emission measurements from the JET vertical SXR camera channels close to the magnetic axis (see in Fig. 3 SXR_{V13} signal) were aligned to the sawtooth crashes. Impurity emission increased monotonically in between sawtooth crashes, slowly levelling off towards the end of the sawtooth cycle. The SXR emission close to the sawtooth inversion radius (r/a ≈ 0.16) (see in Fig.3 SXR_{V08} signal) was higher during the sawtooth crash in comparison to central SXR emission. As an additional observation, the MHD behaviour was quite different for the analyzed pulses. Apart from the sawtooth instabilities, more perturbations of the MHD activity show up regularly during the sawtooth cycle. In the JPN 90758 with +π/2 phasing, as it is presented in Figure 4, core localized Toroidal Alfén Eigenmodes (TAE) with high frequency of 310-340 kHz were excited. TAE excitation is a clear evidence for the generation of energetic ^{3}He ions with ICRH. Also fishbones (FB) activity with wide frequency span was observed indicating a large hot-particle pressure gradient. In between sawtooth crash sawtooth-triggered n=3 and n=2 tearing modes (TM) were observed, while n=1 mode anticipated sawteeth. In the case of discharges with dipole antenna phasing, fishbones with narrow frequency span indicated a weak hot-particle pressure gradient and sawteeth triggered n=3 tearing mode. The discharges with off-axis ICRF was devoid of TAE excitation, fishbones instabilities and sawteeth-triggered tearing modes. As it can be seen in Fig. 3 and Fig. 5 that shows the tomographic reconstruction of the signals detected by the JET bolometry diagnostic [7] for JPN 90752 and JPN 90758,

the total radiated and the $P_{rad,\ bulk}$ were higher in dipole case and most of the radiation came from the bulk plasma. In the cases with the $+\pi/2$ antenna phasing the $P_{rad,\ bulk}$ was slightly reduced, however divertor radiation increased. The impurities were shown to be concentrated mainly around the mid-radius region, where radiation was dominated by W impurity and close to the plasma edge, where high Ni emission was observed.

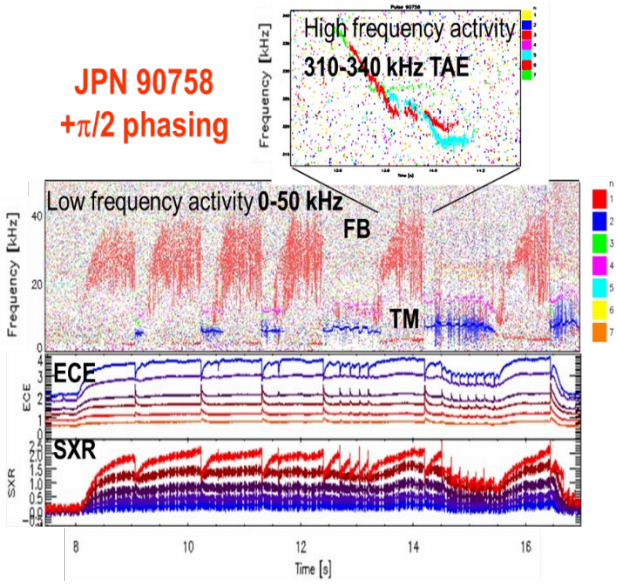

FIGURE 4. MHD activities (Toroidal Alfén Eigenmodes (TAE), fishbones (FB), tearing modes (TM)) in the JPN 90758 with $+\pi/2$ antenna phasing in the D-(^{3}He)-H ICRF scenario on JET with the ECE and SXR signals.

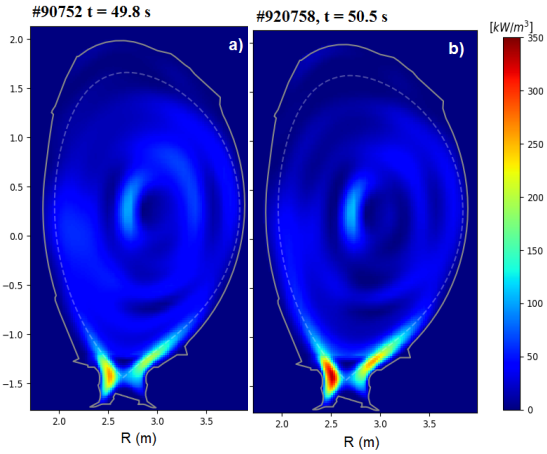

FIGURE 5. Tomographic reconstruction of the radiated power density in between sawtooth crash for JPN 90752 with dipole antenna phasing at t= 9.8 s and JPN 90758 with $+\pi/2$ at 10.5 s.

CONCLUSIONS

The novel 'three-ion' D-(^{3}He)-H minority ICRH heating scheme was tested at JET-ILW. The three-ion scheme heating efficiency was very sensitive to the H:D ratio. For the good ratio (~80%), the absorption was strong and high T_e and low impurity content was obtained at the concentrations of resonant minority ^{3}He ions of the order of ~0.2 % or even below. For the other points the absorption was less good and higher impurity content was observed. Different impurity behaviour in the discharges with dipole and $+\pi/2$ antenna phasing were related to different MHD activities. Such scenario is very promising for both the non-active and DT ITER operational scenarios. The impurity content in L-mode discharges in (^{3}He)-H, (^{3}He)-D and three-ion scheme is similar but it strongly depends on the strike point position.

ACKNOWLEDGMENTS

This work has been carried out within the framework of the EUROfusion Consortium and has received funding from the Euratom research and training programme 2014-2018 and 2019-2020 under grant agreement No 633053. The views and opinions expressed herein do not necessarily reflect those of the European Commission. This scientific work was partly supported by Polish Ministry of Science and Higher Education within the framework of the scientific financial resources in the years 2014-2019 allocated for the realization of the international co-financed project.

REFERENCES

1. E. Lerche et al., Nucl. Fusion **56**, 036022 (2016)
2. Ye. O. Kazakov et al., Nature Physics **13,** 973 (2017)
3. Ye. O. Kazakov et al., Proc. 27th IAEA Fusion Energy Conf., EX/8-1 (2018)
4. T. Putterich et al., Proc. 24rd IAEA Fusion Energy Conf., vol. IAEA-CN-197, EX–P3.15 (2012)
5. A. Czarnecka et al., Plasma Phys. Control. Fusion **53**, 035009 (2011)
6. J. Graves et al., Plasma Phys. Control. Fusion **57**, 014033 (2015)
7. A. Huber et al., Fusion Engineering and Design **82**, 1327 (2007)